International Journal of Engineering Research and Technology. ISSN 0974-3154 Volume 10, Number 1 (2017)

Hydrothermal synthesis of manganese oxide thin films using different oxidizing agents for supercapacitor application

Pragati A. Shinde
Thin Film Physics Laboratory, Department of Physics, Shivaji University, Kolhapur 416 004 (M.S.), India

Vaibhav C. Lokhande
Department of Electronics and Computer Engineering, Chonnam National University, 300 Yongbong-Dong, Puk-Gu, Gwangju 500-757, South Korea

Amar M. Patil
Thin Film Physics Laboratory, Department of Physics, Shivaji University, Kolhapur 416 004 (M.S.), India

Anuja A. Yadav
Thin Film Physics Laboratory, Department of Physics, Shivaji University, Kolhapur 416 004 (M.S.), India.

Prof. Chandrakant D. Lokhande
Professor, Centre for Interdisciplinary Research, D. Y. Patil University, Kolhapur 416 006 (M.S.), India

Abstract
In present work, α-MnO_2, β-MnO_2 and Mn_3O_4 nanostructures are prepared using simple and convenient hydrothermal method. The impact of three different oxidizing agents, on the structural, morphological and electrochemical performance of prepared nanostuctured thin films is investigated. The Mn_3O_4 nanosheets prepared using potassium nitrate as oxidizing agent exhibits excellent electrochemical features such as, high specific capacitance of 1063 F g^{-1} and high energy density of 94.56 Wh kg^{-1} at current density of 1 mA cm^{-2} along with better cycling stability (95% over 1000 of CV cycles). Such an excellent electrochemical properties suggest that Mn_3O_4 nanosheets prepared using hydrothermal method work as significant electrode material for energy storage devices.

Keywords: Hydrothermal method, manganese oxide, nanosheets, oxidizing agents, supercapacitors.

Introduction

The depletion of fossil fuels as well as increase in industrialization along with population are the major issues raised for future generation. To defeat the increasing energy demands of society, significant research attention has been paid in developing effective and clean energy storage devices [1-2]. The supercapacitors also known as electrochemical capacitors (ECs) are energy-storage devices having a specific energy and specific power lying in between batteries and conventional dielectric capacitors [3-5]. Because of their fast energy storage and release features, they are widely used in electric vehicles, renewable energy storage and electronic appliances. The ECs are classified into two types according to their charge storage principle. The first is an electrical double-layer capacitor (EDLC) which utilizes carbon based materials with high surface area and the other is pseudocapacitor which utilizes metal oxides and conducting polymers. The pseudocapacitance is arises due to the capacitive relationship between the level of charge acceptance and the change in the potential from a faradic redox reaction between the electrode material and electrolyte [6-8]. Among the different transition metal oxides used in pseudocapacitors, amorphous and hydrated ruthenium oxide has been reported to show remarkably high specific capacitance compared with other metal oxides [9-10]. However, its commercial use is restricted because of its expensiveness. Therefore, considerable efforts have been devoted to identify cost effective and alternative metal oxide electrode materials with acceptable electrochemical properties.

Manganese oxide is one of the best candidates on account of its electrochemical behavior, low cost, high theoretical specific capacitance and environmental compatibility [11-13]. Manganese oxides have been prepared by different chemical methods including chemical bath deposition [14], electrodeposition [15], SILAR [16], hydrothermal [17], etc. Ma et al. [18] prepared MnO_2 urchin-like hollow spheres which exhibited a specific capacitance of 266.6 F g^{-1} at a current density of 0.1 A g^{-1}. Li et al. [19] synthesized melosira-type MnO_2 with a specific capacitance of 371.2 F g^{-1} at a current density of 0.5 A g^{-1}. Dubal et al. [20] synthesized α-MnO_2 by CBD method which exhibited specific capacitance of 328 F g^{-1}.

In present work, a simple hydrothermal method is employed for the synthesis of manganese oxide nanostructures using different oxidizing agents. The effect of oxidizing agents on structural, morphological and electrochemical properties is investigated. The prepared films are characterized using different characterization techniques. The electrochemical performance is tested in three-electrode cell using battery cycler.

2. Experimental details

2.1 Chemicals

All chemical reagents are analytically pure and used as

received without further purification. $KMnO_4$, $MnSO_4$, $(NH_4)_2S_2O_8$, KNO_3, Polyvinylidene fluoride and N-Methyl-2-pyrrolidone (NMP) were purchased from SD fine chemicals. Double distilled water (DDW) was used for the preparation of precursor solutions.

2.2 Preparation of α-MnO_2, β-MnO_2, Mn_3O_4 samples

In a typical synthesis procedure of α-MnO_2, 0.1 M $MnSO_4$ and 0.1 M $KMnO_4$ (PPM) were mixed in 150 ml of DDW under constant magnetically stirring for 30 min to form a homogeneous mixture. Then, the above mixture was transferred into a Teflon-lined stainless steel autoclave with capacity of 200 ml and heated in oven at 453 K for 12 h. When the autoclave was cooled down to room temperature naturally, the product was collected, washed several times with DDW. Finally, the products were dried in air at 65 °C for 5 h. Similarly, β-MnO_2 samples were obtained from 0.1 M $MnSO_4$ and 0.1 M $(NH_4)_2S_2O_8$ (APS) and Mn_3O_4 samples were obtained from the 0.1 M $MnSO_4$ and 0.1 KNO_3 (PN) in the similar manner as above.

The working electrodes were prepared by the mixing α-MnO_2/β-MnO_2/Mn_3O_4, Polyvinylidene fluoride and N-Methyl-2-pyrrolidone (NMP) with a weight ratio of 85:5:10 uniformly in an agate mortar. The prepared slurry is brush painted on stainless steel (SS) substrate of about 1 cm^2 area. Finally, the electrodes were dried at 338 K for 12 h and used for further characterizations.

2.3 Materials Characterization

The crystallographic study of prepared thin films was carried out by XRD technique using Bruker AXS D8 advance model with copper radiation (Kα λ = 1.54 A). The scanning electron microscopy (SEM) was used to visualize the morphology of thin films. The electrochemical measurements were carried out using automatic battery cycler WBCS 3000 in a conventional three electrode system with 1 M Na_2SO_4 as an electrolyte, WO_3 film as a working electrode, platinum as a counter electrode and saturated calomel electrode (SCE) as a reference electrode.

3. Results and Discussion

The hydrothermal method is based on the controlled precipitation through closed system heating and formation of solid phase on transformation of supersaturated state to saturated state of solution [21]. This transformation process contributes different steps such as initial nucleation, aggregation, coalescence and finally growth of particles. In nucleation, the heterogeneous reactions takes place in the solution and cluster of molecules are formed. Further, the aggregation of particles takes place on the nucleation centres. The coalescence of aggregated particles occurs through Ostwald ripening mechanism [22]. The newly formed nuclei grow on the crystal growth sites and further manganese oxide material is formed. In the present study different manganese oxide samples are synthesized by the direct oxidation of Mn^{2+} species by different oxidizing agents (PPM, APS and PN). The possible chemical reaction for the formation of manganese oxide crystal is given by the following equations;

$$MnSO_4 + (NH_4)_2S_2O_8 + 2H_2O \rightarrow MnO_2 + (NH_4)_2SO_4 + 2H_2SO_4 \quad (1)$$

$$3MnSO_4 + 2KMnO_4 + 2H_2O \rightarrow 5MnO_2 + K_2SO_4 + 2H_2SO_4 \quad (2)$$

$$3MnSO_4 + 2KNO_3 + 4H_2O \rightarrow Mn_3O_4 + K_2SO_4 + 2NO_3 + 4H_2SO_4 \quad (3)$$

The schematic illustration for the growth mechanism of three different manganese oxide nanostructures is shown in fig. 1. When the $MnSO_4$ salt is dissolved in water, Mn^{2+} ions are formed. As the reaction time proceeds, bath solution achieved certain desired temperature. The Mn^{2+} ions are subsequently oxidized by the different oxidizing agents (PPM, APS and PN) and grow as small MnO_2 nanostructures as shown in fig. 1. The crystallinity of the product gradually increases with increase in reaction time. According to the Ostwald ripening mechanism, small crystallites are initially formed in the solution which subsequently grows to form a large particles.

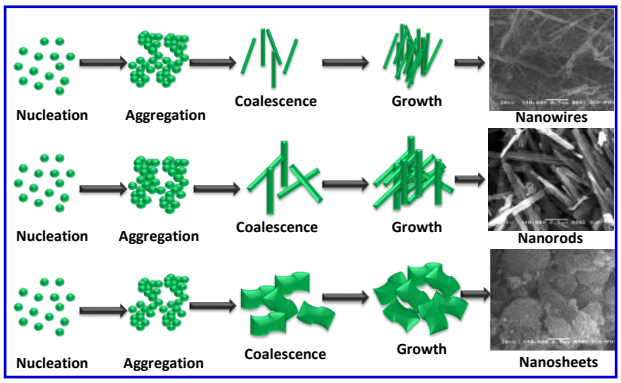

Figure 1: Schematic representation of the formation of α-MnO_2, β-MnO_2 and Mn_3O_4 nanostructues using different oxidizing agents

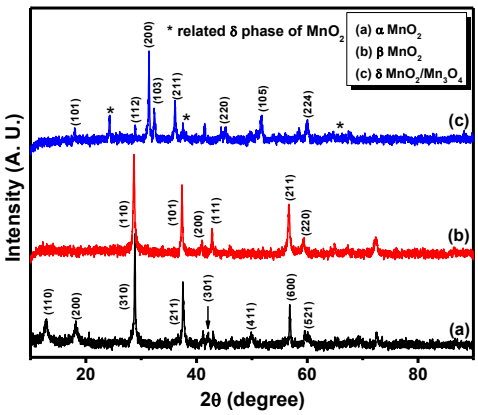

Figure 2: The XRD patterns of a) α-MnO_2, b) β-MnO_2 and c) Mn_3O_4 thin films

The phase structure of MnO_2 thin films is examined by XRD analysis. Fig. 2 exhibits the XRD patterns of (a) α-MnO_2, (b) β-MnO_2 and (c) Mn_3O_4 thin films prepared using different oxidizing agents. The sample prepared using PPM as a oxidizing agent is identified to be tetragonal α-MnO_2 phase (JCPDS 44-0141) as shown in fig. 2(a). The XRD pattern in fig. 2(b) prepared using APS as oxidizing agent shows the formation of tetragonal β-MnO_2 phase (JCPDS 24-0735). The observed diffraction patterns for α-MnO_2 and β-MnO_2 can be

well matches to the earlier reported by Su et al. [17]. Further, fig. 2(c) reveals the formation of tetragonal Mn_3O_4 phase (JCPDS 24-0734). The absence of other diffraction peaks in the XRD patterns reveals pure phase formation of prepared samples. Also the sharp and intense peaks indicate good crystallinity of prepared samples.

As known that, the performance of active electrode material is strongly depends on the morphology of electrode material. The SEM analysis is used to visualize the change in microstructure of α-MnO_2, β-MnO_2 and Mn_3O_4 thin films as a consequence of different oxidizing agents. The surface morphologies of prepared films on SS substrate at two different magnifications of 10,000 X and 40,000 X are shown in fig. 3. The α-MnO_2 thin film demonstrates the nanowires-like surface morphology as shown in fig. 2(A-B). The nanowires have length ~1 μm and diameter below 10 nm. The surface morphology of β-MnO_2 thin film exhibits the formation of randomly distributed nanorods as shown in fig. 3(C-D). The nanorods have lenghth ~1-2 μm and diameter upto 100 nm. The materials with nanostructured morphology enhances the specific surface area as well as ordered pore size distribution permit easy adsorption/desorption of electrolyte ions, which subsequently improves the electrochemical performance of electrode. The surface morphology of Mn_3O_4 shows the formation of randomly oriented porous nanosheets (fig. 3(E-F)). The porous morphology is more favorable for supercapacitors, as it provides the large surface area for easy contact with electrolyte ions, store more charges and produces high specific capacitance.

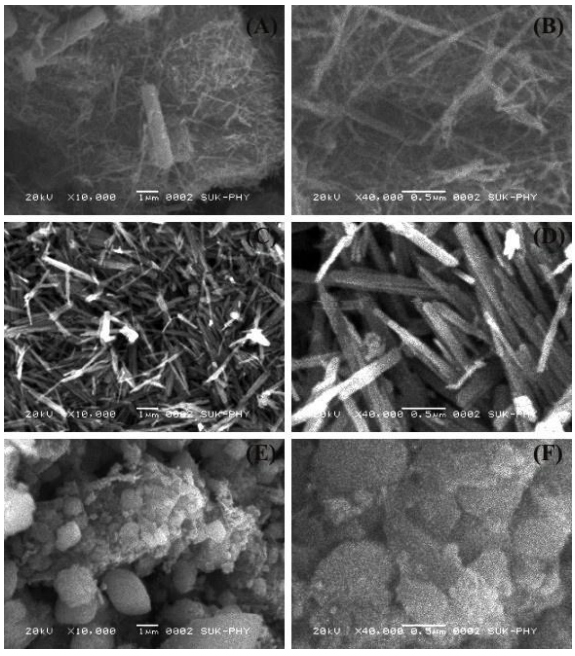

Figure 3: The SEM images of A-B) α-MnO_2, C-D) β-MnO_2 and E-F) Mn_3O_4 thin films at two different magnifications of 10,000 X and 40,000 X

3.1 Electrochemical studies

The cyclic voltammetry (CV) studies of α-MnO_2, β-MnO_2 and Mn_3O_4 electrodes prepared using PPM, APS and PN as oxidising agents are carried out in 1 M Na_2SO_4 electrolyte at different scan rates (5-100 mV s^{-1}) in the potential window of 0 to +0.8 V/SCE. The CV curve of any material assures its capacitive features. Large magnitudes of current, rectangular type of voltammogram and symmetricity in anodic and cathodic directions are implications of the ideal capacitive nature of material. The anodic peak is due to the oxidation of MnO_2/Mn_3O_4 and the cathodic peak is for the reverse process. The MnO_2/Mn_3O_4 electrodes store charges through faradaic ractions occurring at the surface or in the bulk of material.

Fig. 4 (A-C) shows the typical CV curves of α-MnO_2, β-MnO_2 and Mn_3O_4 electrodes at different scan rates. It is seen that, area under the CV curves increases gradually with increase in scan rate. The absence of redox peaks indicates the charge-discharge process at a constant rate over entire potential window [23].

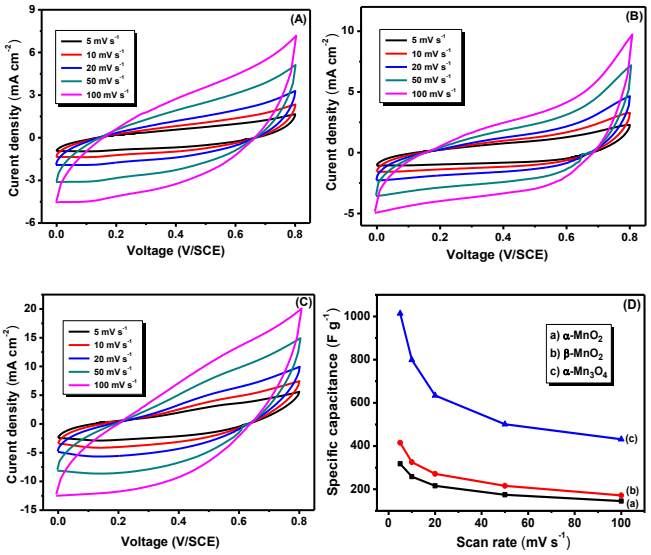

Figure 4: The CV curves of A) α-MnO_2, B) β-MnO_2 and C) Mn_3O_4 electrodes and (D) plot of variation of specific capacitance with scan rate

The specific capacitance is calculated by using the following formula.

$$C_s = \frac{1}{mv(V_{max} - V_{min})} \int_{V_{min}}^{V_{max}} I(V)dv \qquad (4)$$

where, C_s is the specific capacitance, m is the mass of deposited material, $V_{max} - V_{min}$ is the potential window, I is the average current for unit area dipped in the electrolyte. The obtained values of specific capacitance as a function of scan rate are shown in fig. 4(D). The specific capacitance decreases gradually with increase in scan rate. This is because at lower scan rate electrolyte ions take more time for electrochemical reactions and utilizes maximum surface of active material which resulting in higher specific capacitance. The α-MnO_2, β-MnO_2 and Mn_3O_4 electrodes showed the maximum specific capacitance of 318, 415, and 1014 F g^{-1}, respectively at 5 mV s^{-1} scan rate. The maximum values of specific capacitance for Mn_3O_4 electrode prepared using PN, owing to its porous and fine nanosheets structure composed of very fine nanoparticles, which in turns offer the large number of electrochemically active sites for electrochemical reactions.

Further, in order to evaluate specific capacitance and the rate capability of α-MnO_2, β-MnO_2 and Mn_3O_4 electrodes, the galvanostatic charge discharge (GCD) measurements were performed. Fig. 5 (A-C) shows the GCD curves of α-MnO_2, β-MnO_2 and Mn_3O_4 electrodes in 1 M Na_2SO_4 at different current densities (1-4 mA cm^{-1}) using PPM, APS and PN as a oxidizing agents, respectively. The non-linear behaviour of charging and discharging curves reveals the pseudocapacitive behaviour of prepared electrodes.

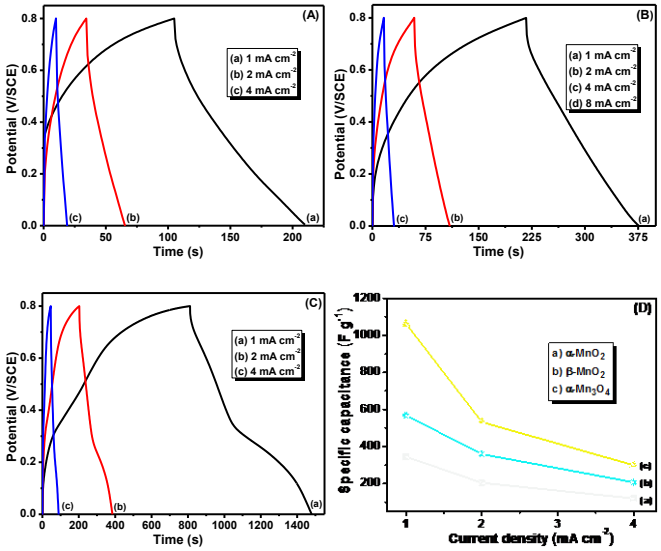

Figure 5: The GCD curves of A) α-MnO_2, B) β-MnO_2 and C) Mn_3O_4 electrodes and (D) plot of variation of specific capacitance with current density

The C_s from GCD curves is calculated using following formula:

$$C_s = \frac{I_d \times T_d}{\Delta V \times m} \tag{5}$$

where, I_d is the discharge current, T_d is the discharge time and ΔV is the potential window. The estimated values of specific capacitance with respect to current densities are plotted in fig. 5(D). The specific capacitance values for α-MnO_2, β-MnO_2 and Mn_3O_4 electrodes are found to be 345, 568 and 1064 F g^{-1}, respectively at 1 mA cm^{-2}.

The energy density (ED) and power density (PD) for are evaluated from discharging curves at different current densities using following formulae.

$$ED = \frac{0.5 \times C_s \times (V^2_{max} - V^2_{min})}{3.6} \tag{6}$$

and

$$PD = \frac{ED \times 3600}{T_d} \tag{7}$$

Ragone plots, demonstrating the relationship between power densities (PD) and energy densities (ED), are employed in order to estimate the operational performance/efficiency of α-MnO_2, β-MnO_2 and Mn_3O_4 electrodes for electrochemical supercapacitor device. The Ragone plots of ED verses PD for α-MnO_2, β-MnO_2 and Mn_3O_4 electrodes are shown in fig. 6. The plots illustrate that α-MnO_2, β-MnO_2 and Mn_3O_4 electrodes exhibits superior energy density which offers excellent electrochemical supercapacitive performance.

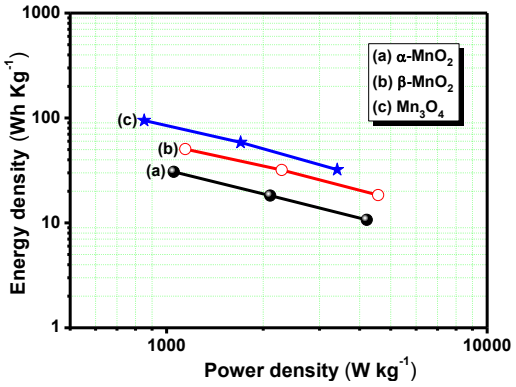

Figure 6: Ragone plots of energy density versus power density for (a) α-MnO_2, b) β-MnO_2 and c) Mn_3O_4 electrodes

Furthermore, the supercapacitor application demands better cycling stability along with superior specific capacitance, energy and power densities, therefore the cycling stability of the α-MnO_2, β-MnO_2 and Mn_3O_4 electrodes is measured in 1 M Na_2SO_4 electrolyte using CV measurement for 1,000 cycles. The CV curves of α-MnO_2, β-MnO_2 and Mn_3O_4 electrodes for different cycles are shown in the fig. 7[A-C]. The variation of capacity retention with cycle number is demonstrated in fig. 7[D]. The remained capacitive retention after 1,000 CV cycles is 90, 92 and 95 % for α-MnO_2, β-MnO_2 and Mn_3O_4 electrodes. The slight loss in capacitance may be due to the dissolution of active material in the electrolyte during the earlier charging/discharging cycles.

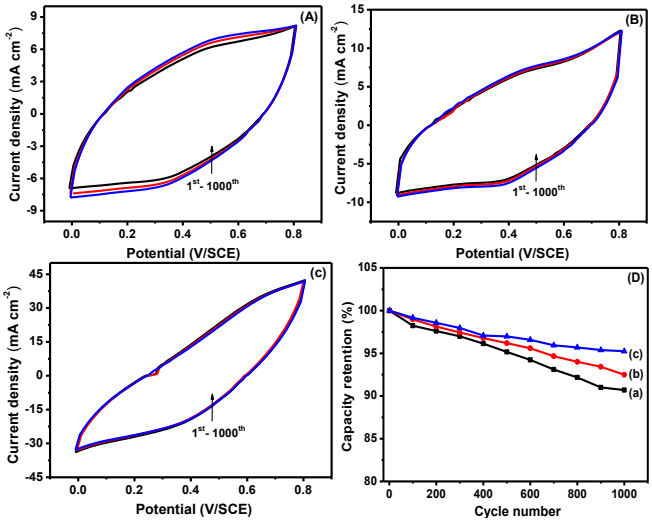

Figure 7: The CV curves of A) α-MnO_2, B) β-MnO_2 and C) Mn_3O_4 electrodes for 1st to 1000th cycles and (D) plot of capacity retention with cycle number.

4. Conclusions

In summary, nanostructured manganese oxide samples are prepared using single step hydrothermal method. The effect of different oxidizing agents (PPM, APS and PN), on structural, morphological and electrochemical performances of manganese oxide thin films is successfully studied. The electrochemical investigation exhibited that, Mn_3O_4 thin film with nanosheets-like morphology possess excellent electrochemical features with high specific capacitance (1014 F g^{-1}), high energy density (94.56 Wh kg^{-1}) and better cycle life (95% over 1000 of CV cycles). The present research work gives the advantageous impact of different oxidizing agents on manganese oxide based electrodes for high performance supercapacitors. Also, it provides simple way for the production of next generation energy storage devices.

Acknowledgement

Authors are also grateful to Department of Science and Technology (DST) Govt. of india for providing financial support through major research project EMR/2016/001677 dated January 13, 2017.

References

[1] J. Liu, J. Jiang, C. Cheng, H. Li , J. Zhang, H. Gong, and H. J. Fan. "Co_3O_4 Nanowire@MnO_2 Ultrathin Nanosheet Core/Shell Arrays: A New Class of High-Performance Pseudocapacitive Materials", Adv. Mater., vol. 23, pp. 2076-2081, 2011.

[2] Y. S. Li, I. W. Sun, J. K. Chang, C. J. Sua and M. T. Lee. "Doped butylmethylpyrrolidinium–dicyanamide ionic liquid as an electrolyte for MnO_2 supercapacitors", J. Mater. Chem., vol. 22, pp. 6274-6279, 2012.

[3] M. Huang, F. Li, F. Dong, Y. X. Zhang, and L. L. Zhang. "MnO_2-based nanostructures for high-performance supercapacitors", J. Mater. Chem. A, vol. 3, pp. 21380-21423, 2015.

[4] Q. Yang, R. Bi, K. Yung, M. Pecht. "Electrochemically reduced 2210rapheme oxides/nanostructured iron oxides as binder-free electrodes for supercapacitors", Electrochim. Acta, vol. 231, pp. 125-134, 2017.

[5] P. A. Shinde, N. R. Chodankar, V. C. Lokhande, A. M. Patil, T. Ji, J. H. Kim and C. D. Lokhande. "Fabrication of high performance flexible all-solidstate asymmetric supercapacitors with a three dimensional disc-like WO_3/stainless steel electrode", RSC Adv., vol. 6, pp. 113442-113451, 2016.

[6] A. D. Jagadale, V. S. Kumbhar, D. S. Dhawale and C. D. Lokhande. "Potentiodynamically deposited nickel oxide (NiO) nanoflakes for pseudocapacitors", J. Electroanal. Chem., vol. 704, pp. 90-95, 2013.

[7] T. Xiao, X. Hu, B. Heng, X. Chen, W. Huang, W. Tao, H. Wang, Y. Tang, X. Tan, and X. Huang. "$Ni(OH)_2$ nanosheets grown on 2210grapheme-coated nickel foam for high-performance pseudocapacitors", J. Alloys Compd., vol. 549, pp. 147-151 (2013).

[8] L. Lina, S. Tanga, S. Zhao, X. Peng, and N. Hu. "Hierarchical three-dimensional $FeCo_2O_4$@MnO_2 core-shell nanosheet arrays on nickel foam for high-performance supercapacitor", Electrochim. Acta, vol. 228, pp. 175-182, 2017.

[9] U. M. Patil, S. B. Kulkarni, V. S. Jamadade and C. D. Lokhande. "Chemically synthesized hydrous RuO_2 thin films for supercapacitor application", J. Alloys Compd., vol. 509, pp. 1677-1682 (2011).

[10] A. Devadas, S. Baranton, T. W. Napporn, and C. Coutanceau. "Tailoring of RuO_2 nanoparticles by microwave assisted Instant method for energy storage applications", J. Power Sources, vol. 196, pp. 4044-4053, 2011.

[11] N. R. Chodankar, D. P. Dubal, G. S. Gund and C. D. Lokhande. "Flexible all-solid-state MnO_2 thin films based symmetric supercapacitors", Electrochim. Acta, vol. 165, pp. 338-347, 2015.

[12] Y. Tian, Z. Liu, R. Xue and L. Huang. "An efficient supercapacitor of three-dimensional MnO_2 film prepared by chemical bath method", J. Alloys Compd., vol. 671, pp. 312-317, 2016.

[13] C. Wei, P. S. Leea and Z. Xu. "A comparison of carbon supports in MnO_2/C supercapacitors", RSC Adv., vol. 4, pp. 31416-31423, 2014.

[14] D. Yan, Z. Guo, G. Zhu, H. Yang, R. Wei, H. Xu, and A. Yu. "Electrochemical properties of 3D MnO_2 film prepared by chemical bath deposition at room temperature", Mater. Lett., vol. 82, pp. 156-158, 2012.

[15] Y. Qiu, P. Xu, B. Guo, Z. Cheng, H. Fan, M. Yang, X. Yang, J. Li. "Electrodeposition of Manganese Dioxide Film on Activated Carbon Paper and Application for Supercapacitor with High Rate Capability", RSC Adv., vol. 4, pp. 64187-64192, 2014.

[16] M. Jana, S. Saha, P. Samanta, N. C. Murmu, N. H. Kim, T. Kuila and J. H. Lee. "A successive ionic layer adsorption and reaction (SILAR) method to fabricate a layer-by-layer (LbL) MnO_2-reduced graphene oxide assembly for supercapacitor application", J. Power Sources, vol. 340, pp. 380-392, 2017.

[17] D. Su, H. J. Ahn and G. Wang. "Hydrothermal synthesis of a-MnO_2 and b-MnO_2 nanorods as high capacity cathode materials for sodium ion batteries", J. Mater. Chem. A, vol. 1, pp. 4845-4850, 2013.

[18] J. Ma, Q. Cheng, V. Pavlinek, P. Sahab and C. Li. "Morphology-controllable synthesis of MnO_2 hollow nanospheres and their supercapacitive performance", New J. Chem., vol. 37, pp. 722-728, 2013.

[19] F. Li, Y. Xing, M. Huang, K. L. Li, T. Ting Yu, Y. X. Zhang and D. Losic. "MnO_2 nanostructures with three-dimensional (3D) morphology replicated from diatoms for highperformance supercapacitors", J. Mater. Chem. A, vol. 3, pp. 7855-7861, 2015.

[20] D. P. Dubal, R. Holze and P. M. Kulal. "Enhanced supercapacitive performances of hierarchical porous nanostructure assembled from ultrathin MnO_2 nanoflakes", J. Mater Sci., vol. 48, pp. 714-719, (2013).

[21] G. S. Gund, D. P. Dubal, S. B. Jambure, S. S. Shinde, and C. D. Lokhande, Temperature influence on morphological progress of $Ni(OH)_2$ thin films and its

subsequent effect on electrochemical supercapacitive properties, J. Mater. Chem. A, vol. 1, pp. 4793-4803, 2013.

[22] M. Lin, Z. Y. Fu, H. R. Tan, J. P. Y. Tan, S. C. Ng, and E. Teo. "Hydrothermal Synthesis of CeO_2 Nanocrystals: Ostwald Ripening or Oriented Attachment", Cryst. Growth Des., vol. 12, pp. 3296-3303, 2012.

[23] Q. Li, X. F. Lu, H. Xu, Y. X. Tong, and G. R. Li. "Carbon/MnO_2 Double-Walled Nanotube Arrays with Fast Ion and Electron Transmission for High-Performance Supercapacitors", ACS Appl. Mater. Interfaces, vol. 6, pp. 2726-2733, 2014.